



Experimental measurements of the radiation characteristics of *Anabaena variabilis* ATCC 29413-U and *Rhodobacter sphaeroides* ATCC 49419

Halil Berberoglu, Laurent Pilon*

Mechanical and Aerospace Engineering Department, Henry Samueli School of Engineering and Applied Science,
University of California Los Angeles, Los Angeles, CA 90095, USA

Received 19 February 2007; received in revised form 10 August 2007; accepted 31 August 2007
Available online 1 November 2007

Abstract

The objective of this study is to experimentally measure the radiation characteristics of hydrogen producing microorganisms. Special attention is paid to the filamentous cyanobacteria *Anabaena variabilis* ATCC 29413-U and the unicellular purple bacteria *Rhodobacter sphaeroides* ATCC 49419 two of the widely studied photobiological hydrogen producers. The extinction and absorption coefficients are measured in the spectral range from 300 to 1300 nm using a spectrophotometer with and without an integrating sphere. Moreover, a nephelometer has been constructed to measure the scattering phase function of the microorganisms at 632.8 nm. The data are used to recover the mass specific absorption, scattering, and extinction cross-sections, the single scattering albedo, and the scattering phase function of the microorganisms. The scattering phase functions of both microorganisms were peaked strongly in the forward direction as expected from their size parameter and shape. The results reported in this study can be used with the radiative transport equation (RTE) to accurately predict and optimize light transport in photobioreactors for photobiological hydrogen production. Finally, the results show that absorption cross-sections of *A. variabilis* and *R. sphaeroides* have peaks that do not overlap but rather enlarge the spectral width of the absorption cross-section of a potential symbiotic culture promising more efficient utilization of solar radiation from light transfer point of view.

© 2007 International Association for Hydrogen Energy. Published by Elsevier Ltd. All rights reserved.

Keywords: Algae; Cyanobacteria; Purple bacteria; Radiation characteristics; Optical properties; Light transfer; Photobioreactor; Photobiological hydrogen production

1. Introduction

Photobioreactors are enclosures used for cultivating microorganisms that utilize light as their energy source for their growth and subsequent product formation [1]. Traditionally, they have been used for a wide range of applications including production of pharmaceuticals, food additives for humans, feed for animals, and cosmetic chemicals [2]. They also find applications in environmental engineering such as wastewater treatment, heavy metal removal, and CO₂ mitigation [2]. More recently, they have been considered for hydrogen production [3–7]. The productivity and efficiency of photobioreactors are mainly limited by light transfer [8–11]. Light transfer within an absorbing and scattering medium, such as a photobioreactor,

is governed by the radiative transport equation (RTE), which is an integro-differential equation expressed in dimensionless optical coordinates [12],

$$\frac{dI_\lambda}{d\tau_\lambda} = -I_\lambda(\tau_\lambda, \hat{s}) + \frac{\omega_\lambda}{4\pi} \int_{4\pi} I_\lambda(\tau_\lambda, \hat{s}_i) \Phi_\lambda(\hat{s}_i, \hat{s}) d\Omega_i, \quad (1)$$

where I_λ is the spectral intensity expressed in W/m²/sr. Here, \hat{s} is the unit vector in the line-of-sight direction and $d\Omega_i$ is the solid angle around the direction \hat{s}_i . The non-dimensional spectral optical thickness τ_λ and single scattering albedo ω_λ are defined, respectively, as

$$\tau_\lambda = \int_0^s (\kappa_\lambda + \sigma_\lambda) ds' = \int_0^s \beta_\lambda ds' \quad (2)$$

and

$$\omega_\lambda = \frac{\sigma_\lambda}{\kappa_\lambda + \sigma_\lambda} = \frac{\sigma_\lambda}{\beta_\lambda}, \quad (3)$$

* Corresponding author. Tel.: +1 310 206 5598; fax: +1 310 206 4830.
E-mail address: pilon@seas.ucla.edu (L. Pilon).

Nomenclature	
$A_{\text{abs},\lambda}$	spectral mass absorption cross-section, m^2/kg
$E_{\text{ext},\lambda}$	spectral mass extinction cross-section, m^2/kg
F	radiation flux, W/m^2
I	intensity, $\text{W}/\text{m}^2/\text{sr}$
L	coordinate direction, Fig. 5(b)
P	pathlength, $P = w/2 \sin \Theta + r$, m
r	the radius of rotation of the fiber-optic probe, m
\hat{s}	local spatial coordinate unit vector
$S_{\text{sca},\lambda}$	spectral mass scattering cross-section of microorganisms, m^2/kg
t	sample thickness, m
T	transmittance, %
U	correction term in recovering the phase function, Eq. (11)
w	incident beam diameter, m
X	microorganism concentration, kg/m^3
z	distance between the detector and the virtual image of the last lens, m
Greek symbols	
β	extinction coefficient, m^{-1}
Θ	scattering angle, rad
κ	absorption coefficient, m^{-1}
λ	wavelength, nm
ω	single scattering albedo
Ω	line-of-sight direction
σ	scattering coefficient, m^{-1}
τ	non-dimensional optical thickness
Φ	scattering phase function
Subscripts	
λ	refers to wavelength
h	refers to hemispherical measurements
PBS	refers to phosphate buffer saline solution
X	refers to microorganism suspension

where κ_λ , σ_λ , and β_λ ($=\kappa_\lambda + \sigma_\lambda$) are the absorption, scattering, and extinction coefficients expressed in m^{-1} , respectively. The scattering phase function $\Phi_\lambda(\hat{s}_i, \hat{s})$ represents the probability of the radiation propagating in direction \hat{s}_i to be scattered in direction \hat{s} , and is normalized such that

$$\frac{1}{4\pi} \int_{4\pi} \Phi_\lambda(\hat{s}_i, \hat{s}) d\Omega_i = 1. \quad (4)$$

Note that the variables κ_λ , σ_λ , β_λ , and Φ_λ are often denoted by a , b , c , and β , respectively, in the ocean optics literature [13]. Eq. (1) indicates that the extinction, absorption, and scattering coefficients together with the scattering phase function and the single scattering albedo are major parameters needed to solve the radiation transfer. Therefore, accurate modeling of light transfer in photobioreactors as well as detecting algal blooms by satellite remote sensing [14], for example require the knowledge of these radiation characteristics.

Moreover, the types of microorganisms commonly used in photobioreactors for hydrogen production include cyanobacteria (or blue-green algae) [6], green algae [15], purple sulfur [16], and purple non-sulfur bacteria [17]. Two of the widely studied photobiological hydrogen producers are the cyanobacteria *Anabaena variabilis* ATCC 29413-U [18] and the purple non-sulfur bacteria *Rhodospira rubra* ATCC 49419 [17,19]. *A. variabilis* is a blue-green microorganism composed of cells of approximately $5 \mu\text{m}$ in diameter forming filaments more than $100 \mu\text{m}$ long. They absorb radiation mainly in the visible part of the electromagnetic spectrum. On the other hand, *R. sphaeroides* is a purple, elliptical shaped unicellular microorganism consisting of cells having equivalent diameters of approximately $1.5 \mu\text{m}$. It absorbs radiation both in the visible and in the near infrared parts of the electromagnetic spectrum. Fig. 1 shows micrographs of *A. variabilis* and *R. sphaeroides* under investigation.

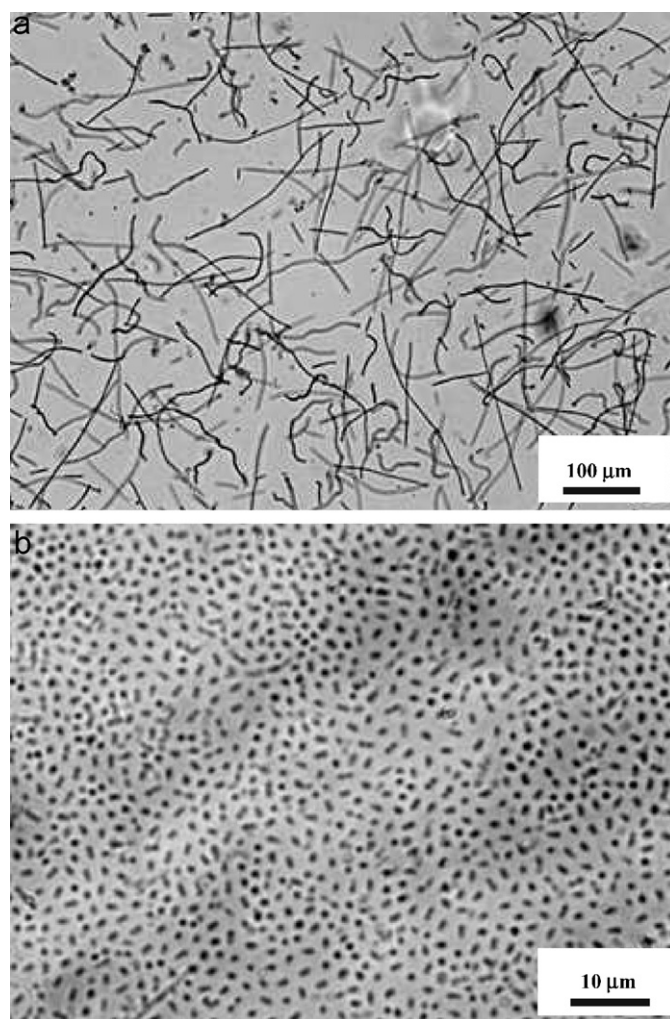


Fig. 1. Micrographs of (a) *A. variabilis* and (b) *R. sphaeroides*.

This study contributes to the development of photobiological production of hydrogen as a sustainable and renewable energy source. More specifically, it aims at determining the radiation characteristics of both the filamentous cyanobacteria *A. variabilis* and the unicellular purple bacteria *R. sphaeroides* over the spectral range from 300 to 1300 nm, where 80% of the solar radiation is concentrated.

2. Current state of knowledge

A comprehensive review of the experimental techniques for measuring the radiation characteristics necessary to solve Eq. (1) has been reported by Agrawal and Mengüç [20]. The absorption and extinction coefficients are linearly proportional to the microorganism concentration if single scattering prevails. Then, they can be used to recover their mass extinction and absorption cross-sections, $E_{\text{ext},\lambda}$ and $A_{\text{abs},\lambda}$, respectively, expressed in m^2/kg and defined as [21]

$$E_{\text{ext},\lambda} = \frac{\beta_\lambda}{X} \quad \text{and} \quad A_{\text{abs},\lambda} = \frac{\kappa_\lambda}{X}, \quad (5)$$

where X is the concentration of the microorganisms, expressed in kg dry cell weight per m^3 of liquid medium, or simply in kg/m^3 , and β_λ and κ_λ are the measured extinction and absorption coefficients of the microorganisms expressed in m^{-1} , respectively. These coefficients and cross-sections can then be used to determine the scattering coefficient σ_λ and the mass scattering cross-section $S_{\text{sca},\lambda}$ expressed in m^2/kg as

$$\sigma_\lambda = \beta_\lambda - \kappa_\lambda \quad \text{and} \quad S_{\text{sca},\lambda} = \frac{\sigma_\lambda}{X}. \quad (6)$$

First, the extinction coefficient β_λ can be retrieved from normal-normal transmittance measurements using a spectrophotometer [12]. Therefore, care has to be taken to ensure that forward scattered radiation in directions other than the incident direction is eliminated in the measurements [12]. This is complicated by the fact that microorganism suspensions are known to scatter light mainly in the forward direction [21–23]. Alternatively, Daniel et al. [22] measured the extinction coefficient of unicellular green algae *Chlorella Pyrenoidosa* using a fiber-optic detector with a small acceptance angle over the spectral range from 370 to 720 nm. In this technique, the fiber-optic probe was submerged in the absorbing and scattering medium thus, eliminating reflection and refraction by the cuvette. Another simple technique for measuring the extinction coefficient of scattering samples consists of focusing the collimated light passing through the sample through a pinhole in front of the detector [24].

Moreover, the measurement of the absorption coefficient κ_λ of an absorbing and scattering sample can be challenging. Daniel et al. [22] used an integrating sphere, as suggested by Butler [25], to measure the absorption coefficient of unicellular algal suspensions. In this method a significant portion of the forward out-scattered radiation is collected by the integrating sphere and the attenuation in the transmitted radiation is attributed solely to the effect of absorption. More recently, Merzlyak and Naqvi [26] pointed out that, this technique can

give inaccurate results due to the differences in the path lengths of scattered radiation reaching the detector. The authors used a method, originally proposed by Latimer and Eubanks [27], and measured the absorption spectrum of *A. variabilis* over the spectral range from 350 to 800 nm. However, this method is based on the assumptions that scattering is isotropic and independent of wavelength. These assumptions are strictly not valid for algal and cyanobacterial suspensions which are known to scatter light mainly in the forward direction and whose radiation characteristics are strongly wavelength dependent and varies based on the photosynthetic process [21,22]. Therefore, this method is not considered in the present study. In contrast, the accuracy of the method used by Daniel et al. [22] can be improved by using a dilute suspension and a relatively thin pathlength t to ensure that single scattering prevails, i.e., $\beta_\lambda t < 0.1$ [23].

Previous studies reporting the radiation characteristics and optical properties of microorganisms mostly studied unicellular species [22,23,28,29]. To the best of our knowledge, this study presents for the first time the complete set of radiation characteristics of both the filamentous cyanobacteria *A. variabilis* and the unicellular purple bacteria *R. sphaeroides* over the spectral range from 300 to 1300 nm as well as their scattering phase function at 632.8 nm.

3. Materials and methods

3.1. Microorganism cultivation and sample preparation

First, *A. variabilis* ATCC 29413-U was purchased from the American Type Culture Collection (ATCC) and received in freeze dried form. The culture was activated with 10 mL of sterilized milli-Q water. It was cultivated under aerobic conditions in ATCC medium 616 with irradiance of 2000–3000 lux provided by fluorescent light bulbs (Ecologic by Sylvania, USA). One liter of ATCC medium 616 contained 1.5 g NaNO_3 , 0.04 g K_2HPO_4 , 0.075 g $\text{MgSO}_4 \cdot 7\text{H}_2\text{O}$, 0.036 g $\text{CaCl}_2 \cdot 2\text{H}_2\text{O}$, 6.0 mg citric acid, 6.0 mg ferric ammonium citrate, 0.02 g Na_2CO_3 , 1.0 mg EDTA, and 1.0 mL of trace metal mix A5. One liter of trace metal mix A5 contains 2.86 g H_3BO_3 , 1.81 g $\text{MnCl}_2 \cdot 4\text{H}_2\text{O}$, 0.222 g $\text{ZnSO}_4 \cdot 7\text{H}_2\text{O}$, 0.39 g $\text{Na}_2\text{MoO}_4 \cdot 2\text{H}_2\text{O}$, 0.079 g $\text{CuSO}_4 \cdot 5\text{H}_2\text{O}$, and 49.4 mg $\text{Co}(\text{NO}_3)_3 \cdot 6\text{H}_2\text{O}$. The initial pH of the medium was 7.3.

Moreover, *R. sphaeroides* ATCC 49419 was purchased from ATCC and received in freeze dried form. The culture was activated with ATCC medium 112 containing 2.0% by volume cysteine solution. It was cultivated under aerobic conditions in ATCC medium 112 with irradiance of 2000–3000 lux provided by a tungsten light bulb (Krypton 60 W by Feit Electric, USA). One liter of ATCC medium 112 contains 1.0 g K_2HPO_4 , 0.5 g MgSO_4 , and 10 g yeast extract. The initial pH of the medium was 7.3.

Finally, samples were taken from actively growing cultures of each species during their exponential growth phase. In order to eliminate the absorption and scattering due to the nutrient media, the microorganisms were centrifuged at 2000 rpm for 10 min (Super T21 by Sorvall, USA), washed, and suspended in phosphate buffer saline (PBS) solution. While measuring their radiation characteristics, the microorganisms should not

be suspended in distilled water [30]. Indeed, due to the large osmotic gradient between the inside of the cells and pure water, the cells will absorb water and burst. However, PBS solution overcomes this problem and provides a non-absorbing and non-scattering medium, suitable for optical measurements [30]. One liter of PBS solution contains 8 g NaCl, 0.2 g KCl, 1.15 g $\text{Na}_2\text{HPO}_4 \cdot 7\text{H}_2\text{O}$, and 0.2 g KH_2PO_4 . The pH of the PBS solution was 7.3. Three dilutions of each species were prepared. Microorganism concentration of each dilution was determined using the calibration procedure similar to that reported previously [31]. In brief, the calibration curves relate the optical-density (OD) of microorganism suspensions to the dry cell weight per unit volume of liquid at a particular wavelength. For *A. variabilis* and *R. sphaeroides*, 1 unit of OD using a 1 cm pathlength cuvette corresponds to microorganism concentrations of 0.274 and 0.521 kg/m^3 at the absorption peaks 683 and 800 nm, respectively.

3.2. Experimental setup

First, the extinction coefficients of the microorganisms are estimated from normal-normal transmittance measurements over the spectral range from 300 to 1300 nm using a UV-VIS-NIR

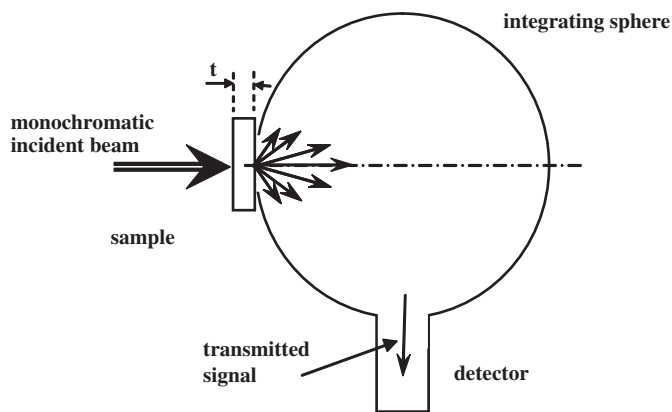


Fig. 2. Setup for determining the absorption coefficient.

spectrophotometer (Shimadzu, USA, Model UV-3101PC). Furthermore, the absorption coefficients are measured using the method described by Daniel et al. [22] and schematically shown in Fig. 2. In this method, an integrating sphere having an internal diameter of 8 cm (ISR-3100 by Shimadzu, USA) is used with the spectrophotometer to collect a significant portion of the scattered radiation, which is mainly in the forward

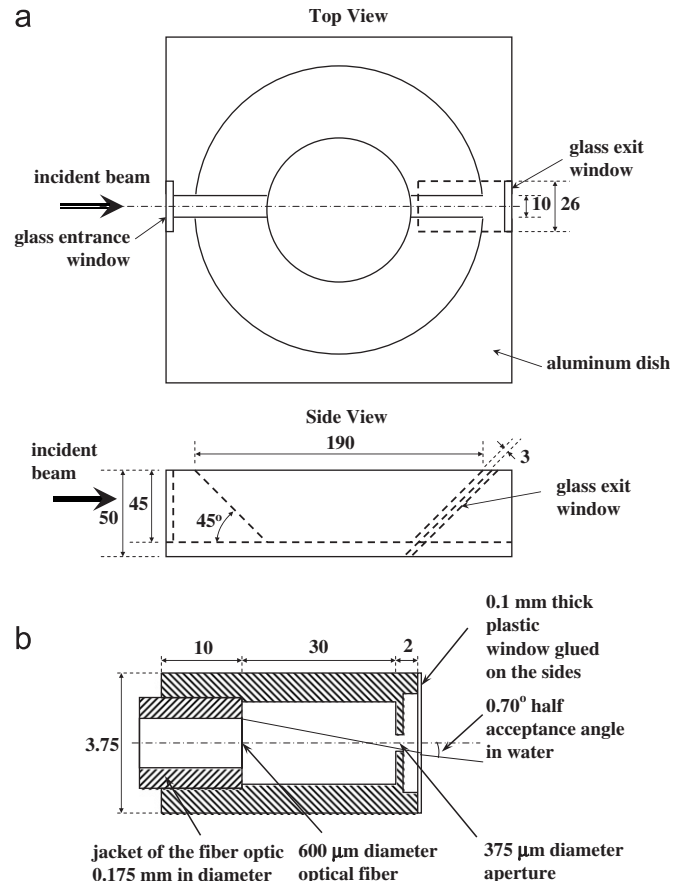


Fig. 4. Construction of (a) the sample holder dish and (b) the miniaturized gershun tube (drawings not to scale). All dimensions are given in mm unless otherwise stated.

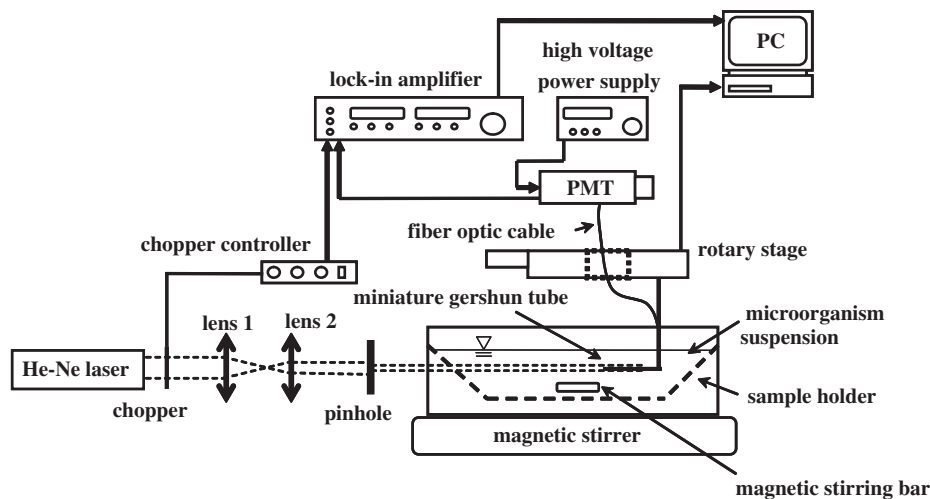


Fig. 3. Schematic of the nephelometer used to measure the scattering phase function at 632.8 nm.

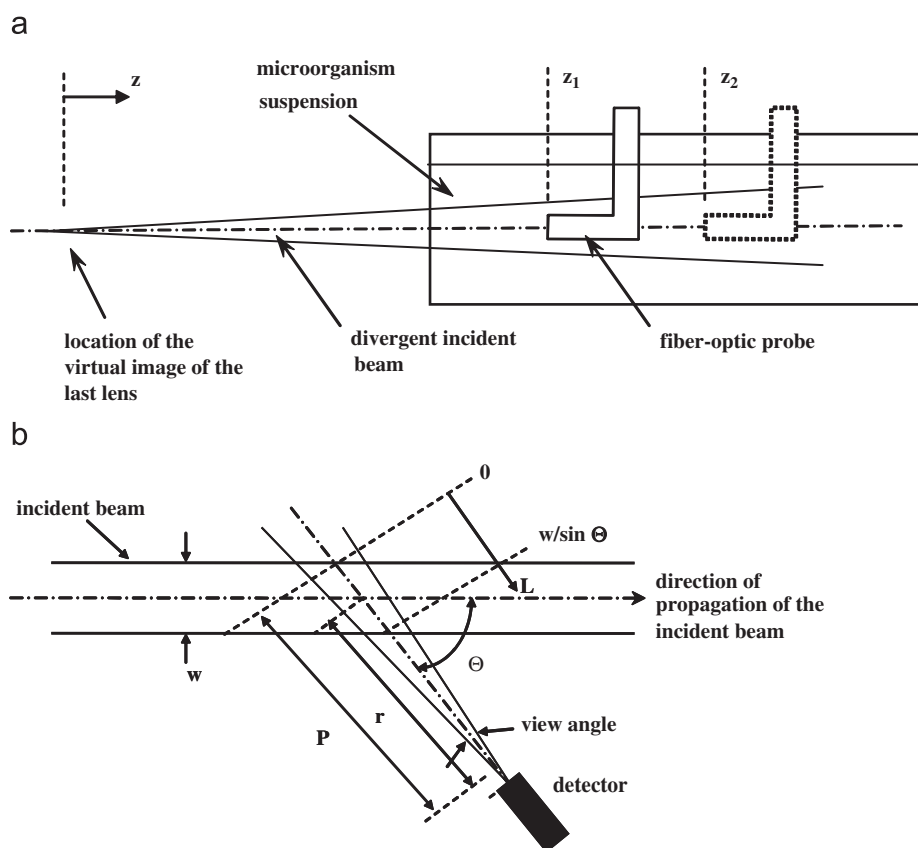


Fig. 5. (a) Setup for measuring the extinction coefficient and (b) coordinate system used in recovering the scattering phase function from the measured intensity distribution.

direction. The inside of the integrating sphere is coated with barium sulfate, a highly reflecting material, to direct the collected radiation to the detector enabling the transmitted radiation in all directions to be measured. Therefore, the attenuation in the incident beam is solely due to absorption by the suspension. All the transmission measurements are carried out in a 100 μm pathlength liquid flow cell with quartz windows (FT04-060 by Thermo, USA). During the measurements, the microorganism suspension is continuously flown through the cell with a peristaltic pump (4049 K33 by McMaster, USA) at a flow rate of approximately 10 mL/min to avoid settling of microorganisms.

Finally, a nephelometer has been constructed to experimentally measure the scattering phase function and the extinction coefficient of microorganisms at 632.8 nm. Fig. 3 shows the schematic of the experimental setup. A He–Ne laser (21-5004 by Ealing Electro-Optics, USA) provides a continuous 15 mW laser beam at 632.8 nm. It is modulated by a beam chopper (SR540 by Stanford Research, USA) at 150 Hz. The modulated beam is collimated and reduced to a diameter of 1.7 mm by a set of collimating lenses and a pinhole. The divergence angle of the beam is 0.046°. Both the beam size and the divergence angle were measured with the knife-edge method [32]. The collimated beam enters a custom made sample holder dish containing the microorganism suspension through a transparent glass window as shown in Fig. 4(a). The dish is made of aluminum and painted with Krylon ultra flat black spray paint. The sides of the dish are banked at 45° to minimize reflections within

the container. The scatterers are kept in suspension with the aid of a black magnetic stirring bar and a magnetic stirrer (Model 131325 by Barnstead Thermolyne, USA). The scattered light is collected with a custom made fiber-optic probe consisting of (i) a miniaturized gershun tube with half acceptance angle of 0.70° and (ii) a solarization resistant UV–IR fiber-optic cable having a core diameter of 600 μm (ZDF-10359 by Ocean Optics, USA). Fig. 4(b) shows the geometry and the dimensions of the gershun tube.

The probe is mounted on a computer controlled motorized rotary stage (MM-4M-R by National Aperture Inc., USA) with an angular resolution of 4.54×10^{-3} degree. Data are collected at 1° increments from 0° to 10° and at 2° increments from 10° to 180°. Due to finite beam diameter, the fiber-optic probe blocks the incident beam at scattering angles greater than 160°. Therefore, data could only be obtained for scattering angles up to 160°. The collected light is detected with a photomultiplier tube (PMT) (R928 by Hamamatsu, USA) and amplified with a lock-in amplifier (SR 830 by Stanford Research, USA). The PMT is powered with a variable high voltage power supply (PS310 by Stanford Research, USA). The latter enables the sensitivity of the PMT to be varied so that the input to the lock-in amplifier is within its detection range. Use of the lock-in amplifier together with the beam chopper enables the detection of noisy signals otherwise difficult to detect. The experimental setup is fully automated with the aid of a LabView program. The program controls and registers the position of the fiber-optic

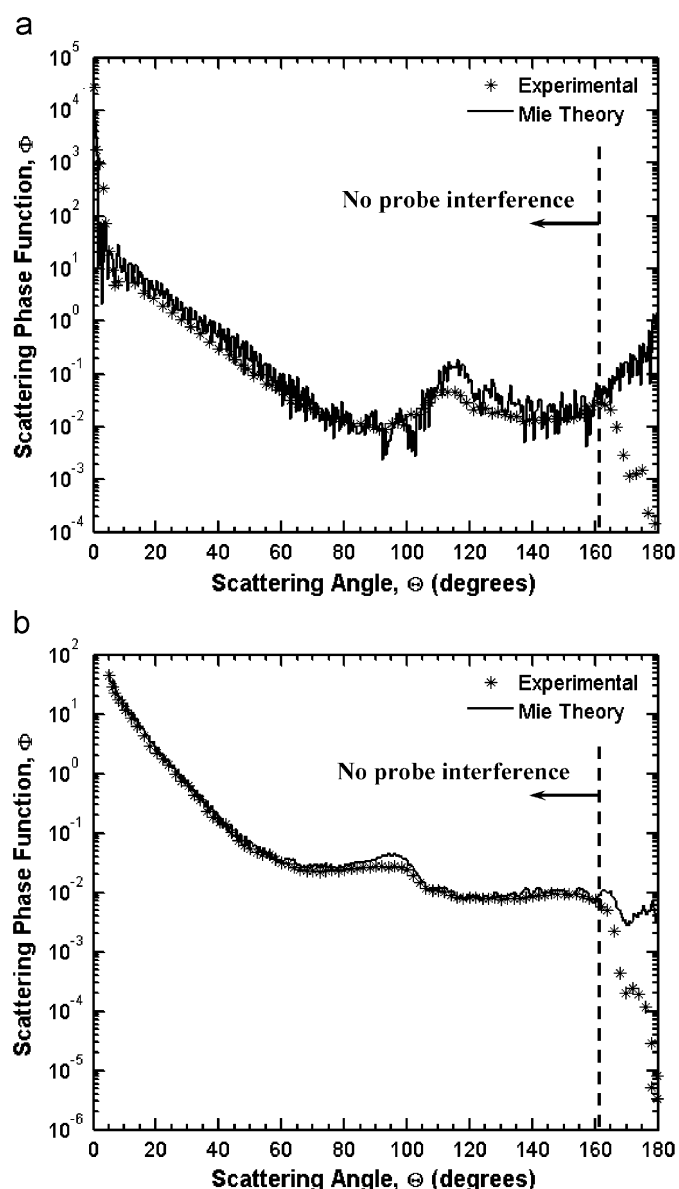


Fig. 6. Comparison of the scattering phase functions of (a) polystyrene spheres and (b) glass fibers obtained experimentally using Eq. (10) and predicted by the Mie theory.

probe, collects the signal from the lock-in amplifier at 10 Hz for 15 s (150 data points), and records the arithmetic mean, the standard deviation, and the standard error of the signal. The data are saved only if the standard error in the measured intensities is at most two orders of magnitude less than the mean value. The standard error is defined as the ratio of the standard deviation to the square root of the number of samples. The present setup is an improved version of that used by Privoznik et al. [23] as it incorporates (1) a magnetic stirrer to keep the microorganisms in suspension and randomly oriented, (2) a lock-in amplifier to enable reliable detection of low and noisy signals, (3) a smaller detector acceptance angle for more precise scattered light measurements, (4) a motorized stage for more precise and repeatable measurements of the scattering angles, and (5) a computer automated operation for faster data acquisition.

3.3. Data analysis and validation

In analyzing the data the following assumptions are made: (1) the microorganisms are well mixed and randomly oriented, (2) for all measurements, the pathlength and the concentration of the samples is such that single scattering prevails, (3) the optical setup of the spectrophotometer sufficiently eliminates the forward scattered light in directions other than the incident direction, (4) the difference in the optical pathlengths of the scattered and transmitted light is negligible, (5) scattering is mainly in the forward direction and all the scattered light can be collected by an integrating sphere, and (6) the scattering phase function has azimuthal symmetry and is only a function of the polar angle.

First, the extinction coefficient β_λ is obtained from the normal-normal transmittance measurements of the samples over the spectral range from 300 to 1300 nm. In order to account for reflection and refraction by the cuvette, measurements are made with respect to the transmission spectrum of PBS alone in the cuvette denoted by $T_{\lambda,PBS}$. Then, the extinction coefficient is given by [24]

$$\beta_\lambda = \frac{1}{t} \ln \left(\frac{T_{\lambda,X}}{T_{\lambda,PBS}} \right), \quad (7)$$

where $T_{\lambda,X}$ is the transmission spectra of the microorganism suspension of concentration X .

Moreover, in order to validate the measurements taken with the spectrophotometer, the extinction coefficient is compared with that measured with the nephelometer at wavelength 632.8 nm. In this method, the radiation flux $F_\lambda(z)$, expressed in W/m^2 , at two different locations z_1 and z_2 along the path of a divergent incident beam are measured. The extinction coefficient is evaluated as [22]

$$\beta_{632.8} = \frac{\ln |F_{632.8}(z_2)/F_{632.8}(z_1)| + \ln |z_1^2/z_2^2|}{z_1 - z_2}, \quad (8)$$

where z is the distance between the detector and the virtual image of the last lens in the optical setup shown in Fig. 5(a). Note that the second term in the numerator accounts for the divergence of the incident beam. The mass extinction cross-sections measured with the two different methods at 632.8 nm fall within 2.5% of each other. This confirms the validity of the retrieval method of β_λ using the spectrophotometer and Eq. (8) at the same wavelength.

Similarly, the absorption coefficient is recovered from the transmittance measurements performed with the integrating sphere as [22]

$$\kappa_{\lambda,X} = \frac{1}{t} \ln \left(\frac{T_{h,\lambda,X}}{T_{h,\lambda,PBS}} \right), \quad (9)$$

where $T_{h,\lambda,X}$ and $T_{h,\lambda,PBS}$ are the normal-hemispherical transmittance of the microorganism suspension and of the PBS solution, respectively. Moreover, the hemispherical reflectance of the samples is measured with the integrating sphere method to evaluate the contribution of the backscattering to the overall attenuation of light by the microorganisms. The data (not shown)

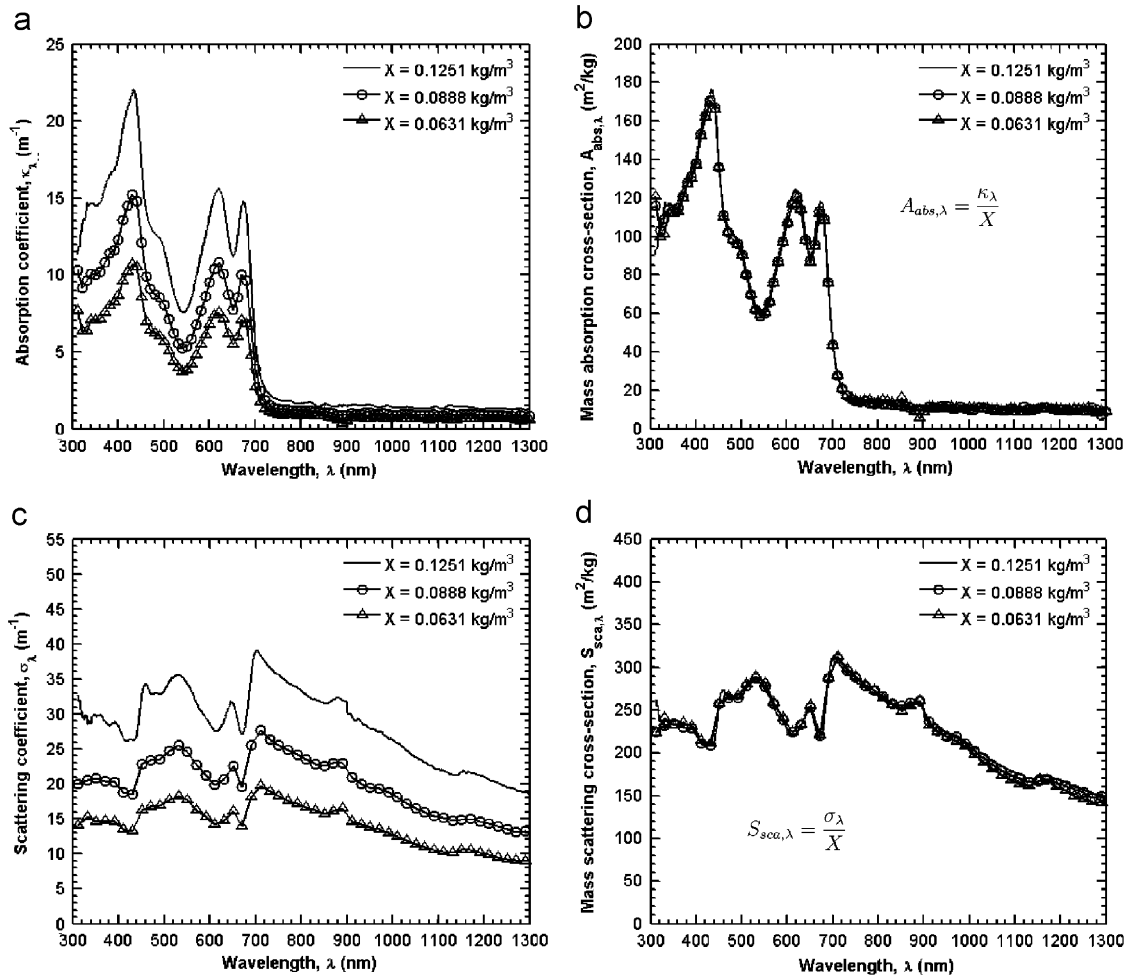


Fig. 7. Spectral (a) absorption and (c) scattering coefficients, and the corresponding (b) mass absorption and (d) mass scattering cross-sections of *A. variabilis* measured at three different microorganism concentrations from 300 to 1300 nm.

indicate that the hemispherical reflectance is less than 4% over the spectral range from 300 to 1300 nm. Thus, backscattering is negligible in recovering the absorption coefficient κ_λ using Eq. (9).

Finally, the constructed nephelometer measures the scattered intensity I_λ in $\text{W}/\text{m}^2/\text{sr}$ as a function of the polar angle θ . The scattering phase function is recovered using the analysis suggested by Daniel et al. [22]

$$\Phi_\lambda(\theta) = \frac{2I_\lambda(\theta)[U_\lambda(\theta)]^{-1}}{\int_0^\pi I_\lambda(\theta)[U_\lambda(\theta)]^{-1} \sin \theta d\theta}. \quad (10)$$

The term $U_\lambda(\theta)$ is a geometrical correction term defined as [22]

$$U_\lambda(\theta) = \int_0^{w/\sin \theta} \left[1 + \beta_\lambda \frac{w}{2} c \tan \theta - \beta_\lambda L \cos \theta \right] \times \left[1 - \beta_\lambda \left(r - \frac{w}{2 \sin \theta} \right) \right] \times \left[1 - \beta_\lambda \left(\frac{w}{\sin \theta} - L \right) \right] dL, \quad (11)$$

where w is the beam diameter in m, r is the radius of rotation of the fiber-optic probe, equal to 6.0×10^{-3} m, and L is

the coordinate direction along the line of sight of the detector, marking the length of the scattering volume as shown in Fig. 5(b). The pathlength of the radiation reaching the detector is denoted by $P = w/2 \sin \theta + r$ [23]. Note that due to the finite size of the probe and the beam, data can only be obtained for scattering angle θ up to 160° where the probe does not block the incident beam. At all angles the value of $\beta_\lambda P$ is less than 0.1 ensuring single scattering [23].

Measurements from the nephelometer and the procedure to analyze the data have been successfully validated using polystyrene microspheres supplied by Duke Scientific Corp., USA (Part No: 7520A). The size distribution of the polystyrene microspheres was measured with Beckman Coulter particle size analyzer LS 13-320. The microspheres are spherical and their size distribution follows a Gaussian distribution with a mean diameter of $19 \mu\text{m}$ and a standard deviation of $3.56 \mu\text{m}$. Their complex refractive index at 632.8 nm is equal to $1.5823 - i4.5 \times 10^{-4}$ [33]. Fig. 6(a) compares the experimentally determined scattering phase function of the microspheres retrieved using Eq. (10) and that predicted by the Mie theory for polystyrene spheres of diameter $19 \mu\text{m}$ [24]. Good agreement is found up to 160° .

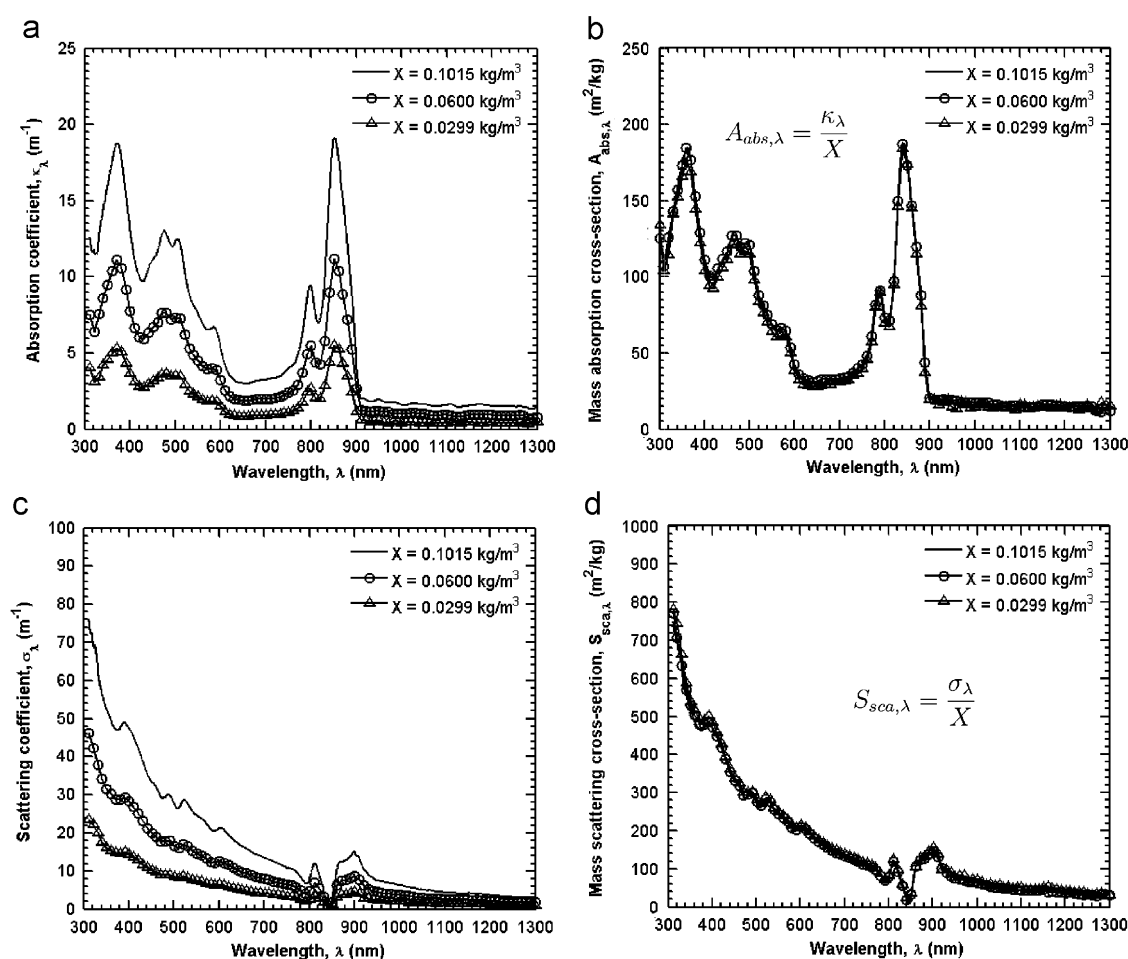


Fig. 8. The spectrum of the (a) absorption and (c) scattering coefficients, and the corresponding (b) mass absorption and (d) mass scattering cross-sections of *R. sphaeroides* measured at three different microorganism concentrations from 300 to 1300 nm.

In addition, the experimental setup and the procedure were also validated using glass microfibers 15–20 μm in diameter and 10 mm in length supplied by A&P Technology, USA (Part No: TA 1940). This validation was carried out to demonstrate the capability of the nephelometer to measure the scattering phase function of randomly oriented filamentous microorganisms such as *A. variabilis*. Unfortunately, the supplier did not specify the glass composition or the optical properties of the fibers. Therefore, as a first order approximation, their complex index of refraction is assumed to be that of silica and equal to $1.4567 - i1 \times 10^{-7}$ at 632.8 nm [34,35]. Fig. 6(b) compares the experimentally determined scattering phase function of the glass fibers and that predicted by the Mie theory for randomly oriented infinitely long cylinders of diameter 17 μm [36]. Here also very good agreement is found between experimental data and Mie theory demonstrating the capability of the nephelometer.

4. Results

First, the extinction and absorption coefficients of *A. variabilis* were measured at three different microorganism concentrations, namely 0.0631, 0.0888, and 0.1251 kg/m^3 in the

spectral region from 300 to 1300 nm. The measurements were performed twice and the arithmetic mean of the results is reported. The relative difference between measurements was less than 2% over the entire spectral range of interest. Similarly, the extinction and absorption coefficients of *R. sphaeroides* were determined at microorganism concentrations of 0.0299, 0.0600, and 0.1015 kg/m^3 . Then, these coefficients were normalized with the respective microorganism concentrations to obtain the mass extinction and absorption cross-sections defined in Eq. (5). Moreover, the scattering coefficient and cross-section, as well as the single scattering albedo were calculated as given by Eqs. (3) and (6). Finally, the scattering phase functions of *A. variabilis* and *R. sphaeroides* are recovered at microorganism concentrations of 0.0035 and 0.0042 kg/m^3 at wavelength 632.8 nm.

Figs. 7(a)–(d), respectively, show the absorption coefficient κ_λ , the mass absorption cross-section $A_{\text{abs},\lambda}$, the scattering coefficient σ_λ , and the mass scattering cross-section $S_{\text{sca},\lambda}$ of *A. variabilis* over the spectral range from 300 to 1300 nm. Figs. 7(a) and (c) show that both the absorption and scattering coefficients increase with increasing microorganism concentration. When these coefficients are normalized with the respective microorganism concentration X , the mass absorption

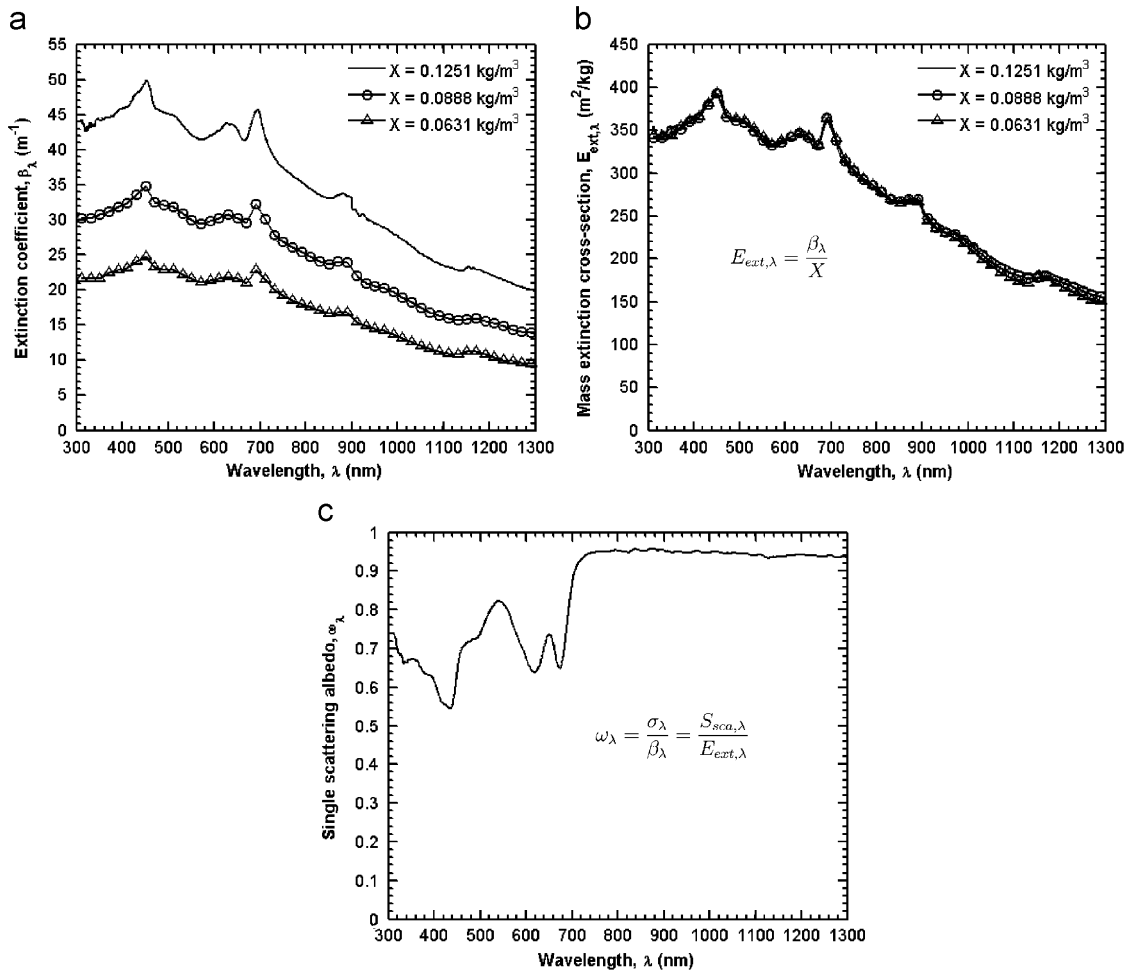


Fig. 9. Spectral (a) extinction coefficients, (b) mass extinction cross-sections, and (c) the average single scattering albedo of *A. variabilis* measured at three different microorganism concentrations from 300 to 1300 nm.

and scattering cross-sections each collapse on a single line, confirming that the cross-sections $A_{\text{abs},\lambda}$ and $S_{\text{sca},\lambda}$ are independent of microorganism concentration, as shown in Figs. 7(b) and (d), respectively. This also confirms that multiple scattering effects are negligible in the experiments. Moreover, Fig. 7(a) shows that *A. variabilis* absorbs mainly in the spectral region from 300 to 700 nm with absorption peaks at 435 and 676 nm, corresponding to those of the light harvesting pigment chlorophyll a, and at 621 nm corresponding to that of the pigment phycocyanin [37]. The values of the absorption cross-section $A_{\text{abs},\lambda}$ at the absorption peaks 435, 621, and 676 nm are 173, 122, and 116 m²/kg, respectively. At wavelengths greater than 700 nm *A. variabilis* does not absorb light appreciably. Furthermore, the small and relatively constant absorption coefficient observed in this spectral region is less than 9.4% of the peak absorption values and can be due to the scattered light that could not be collected with the finite acceptance angle of the integrating sphere. Finally, Fig. 7(d) indicates that the mass scattering cross-section $S_{\text{sca},\lambda}$ of *A. variabilis* varies between 200 and 300 m²/kg over the spectral range from 300 to 700 nm, having local minima at absorption peak wavelengths.

Similarly, Figs. 8(a)–(d) show the absorption coefficient κ_λ , the mass absorption cross-section $A_{\text{abs},\lambda}$, the scattering coefficient σ_λ , and the mass scattering cross-section $S_{\text{sca},\lambda}$ of *R. sphaeroides*, respectively, over the spectral range from 300 to 1300 nm. Here also, the cross-sections obtained for different concentrations of *R. sphaeroides* collapse on a single line as shown in Figs. 8(b) and (d). Moreover, Fig. 8(b) shows that *R. sphaeroides* absorbs mainly in two distinct spectral regions from 300 to 600 nm and from 750 to 900 nm. The major absorption peaks are observed around 370, 480, 790, and 850 nm and can be attributed to the presence of bacteriophyll b and carotenoids in the antenna complexes B850 and the reaction center complex (LM) [37,38]. The values of the absorption cross-section at these peaks are 187, 128, 84, and 188 m²/kg, respectively. Furthermore, at wavelengths greater than 900 nm *R. sphaeroides* does not absorb light appreciably. The relatively constant absorption cross-sections observed in this spectral region have similar magnitude as those of *A. variabilis* and are found to be negligible. Finally, Fig. 8(d) indicates that the scattering cross-section of *R. sphaeroides* varies significantly from about 780 to 30 m²/kg over the spectral range from 300 to 1300 nm displaying an inverse relation with wavelength.

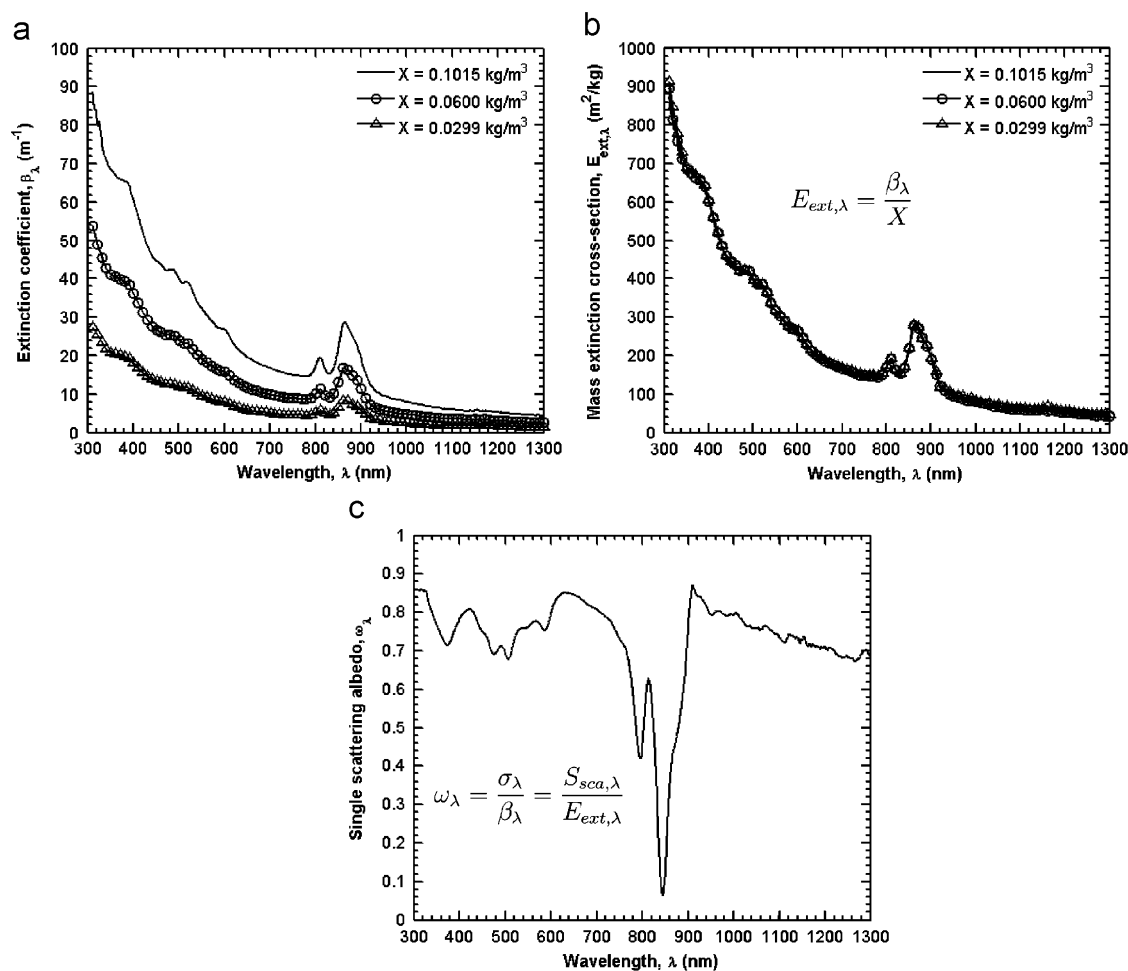


Fig. 10. Spectral (a) extinction coefficients, (b) mass extinction cross-sections, and (c) the average single scattering albedo of *R. sphaeroides* measured at three different microorganism concentrations from 300 to 1300 nm.

Moreover, Figs. 7(b) and 8(b) indicate that the absorption cross-sections of *A. variabilis* and *R. sphaeroides* have peaks that do not overlap but rather enlarge the spectral width of the absorption cross-section of a symbiotic culture. From a light transfer point of view, a photobioreactor cultivating a symbiotic culture with such absorption spectra would have a higher light to hydrogen energy conversion efficiency compared with that of the individual cultures [16]. However, attention has to be paid when choosing the symbiotic culture such that the species are compatible and do not adversely affect each other's hydrogen production rate.

Alternatively, the extinction coefficient β_λ , the mass extinction cross-section $E_{ext,\lambda}$, and the average single scattering albedo ω_λ for *A. variabilis* over the spectral range from 300 to 1300 nm are presented in Figs. 9(a)–(c), respectively. Fig. 9(b) indicates that the extinction cross-section obtained is indeed independent of microorganism concentration. In addition, Fig. 9(c) shows that the average single scattering albedo ω_λ was greater than 0.55 over the PAR. This indicates that scattering is significant and the scattering phase function has to be measured accurately or approximated with an appropriate model such as the Henyey–Greenstein (HG) or the truncated phase function (TPF) [21].

Similarly, Fig. 10 shows the extinction coefficient, the extinction cross-section, and the single scattering albedo of *R. sphaeroides* over the spectral range from 300 to 1300 nm. Fig. 10(c) shows that the single scattering albedo of *R. sphaeroides* is greater than 0.68 over the PAR and at wavelengths greater than 900 nm. However, in the spectral range from 700 to 900 nm it decreases significantly indicating that absorption dominates over scattering. Finally, the cross-sections as well as the single scattering albedo for both *A. variabilis* and *R. sphaeroides* are tabulated in Table 1 over the spectral range from 300 to 1300 nm.

Note that Merzlyak and Naqvi [26] reported the so-called true absorption and scattering spectrum of *A. variabilis* over the spectral range from 350 to 800 nm. However, the authors did not pay attention to eliminate the forward scattered light when measuring the extinction coefficient and therefore obtained smaller values of extinction coefficient than those measured in the present study. As a result, their values of the scattering coefficient are about four times smaller than those in the present study. In the present study, the value of the extinction coefficient was measured at 632.8 nm with two independent techniques and was shown to agree within 2.5% which gives confidence in the results reported here.

Table 1
Radiation characteristics of *A. variabilis* and *R. sphaeroides* in the spectral range from 300 to 1300 nm. The reported data is available in digital format from the corresponding author

λ (nm)	<i>A. variabilis</i>				<i>R. sphaeroides</i>			
	$A_{\text{abs},\lambda}$ (m ² /kg)	$S_{\text{sca},\lambda}$ (m ² /kg)	$E_{\text{ext},\lambda}$ (m ² /kg)	ω	$A_{\text{abs},\lambda}$ (m ² /kg)	$S_{\text{sca},\lambda}$ (m ² /kg)	$E_{\text{ext},\lambda}$ (m ² /kg)	ω
310	109.13	236.20	345.33	0.684	127.67	767.00	894.67	0.857
320	103.00	239.67	342.67	0.699	108.33	714.00	822.33	0.868
330	108.33	235.00	343.33	0.684	121.33	639.33	760.67	0.840
340	114.33	230.00	344.33	0.668	142.00	571.33	713.33	0.801
350	113.67	234.33	348.00	0.673	155.67	526.67	682.33	0.772
360	115.33	238.00	353.33	0.674	170.67	502.67	673.33	0.747
370	122.00	232.33	354.33	0.656	182.67	479.33	662.00	0.724
380	128.67	227.33	356.00	0.639	174.00	479.33	653.33	0.734
390	132.00	230.00	362.00	0.635	149.67	489.33	639.00	0.766
400	139.00	225.67	364.67	0.619	126.33	474.00	600.33	0.790
410	153.67	212.67	366.33	0.581	108.00	450.33	558.33	0.807
420	164.00	210.00	374.00	0.562	97.73	420.60	518.33	0.811
430	171.67	210.00	381.67	0.550	95.70	388.63	484.33	0.802
440	167.67	217.67	385.33	0.565	102.80	354.87	457.67	0.775
450	137.00	257.67	394.67	0.653	109.33	333.00	442.33	0.753
460	111.67	275.00	386.67	0.711	114.33	319.67	434.00	0.737
470	103.00	264.33	367.33	0.720	124.67	295.00	419.67	0.703
480	99.17	264.50	363.67	0.727	124.67	295.67	420.33	0.703
490	97.10	264.90	362.00	0.732	118.00	299.33	417.33	0.717
500	91.33	270.00	361.33	0.747	120.00	276.00	396.00	0.697
510	81.03	278.63	359.67	0.775	118.67	267.33	386.00	0.693
520	70.63	285.03	355.67	0.801	101.60	284.40	386.00	0.737
530	62.87	286.80	349.67	0.820	86.30	275.70	362.00	0.762
540	59.47	285.20	344.67	0.827	79.17	256.50	335.67	0.764
550	60.93	277.73	338.67	0.820	73.27	244.07	317.33	0.769
560	66.80	267.87	334.67	0.800	66.93	235.73	302.67	0.779
570	76.70	255.97	332.67	0.769	63.37	224.63	288.00	0.780
580	87.60	246.73	334.33	0.738	64.63	209.70	274.33	0.764
590	98.00	238.67	336.67	0.709	62.97	204.03	267.00	0.764
600	108.33	230.00	338.33	0.680	52.07	210.93	263.00	0.802
610	118.33	223.67	342.00	0.654	40.70	205.63	246.33	0.835
620	121.67	225.00	346.67	0.649	34.23	193.43	227.67	0.850
630	115.33	232.33	347.67	0.668	31.27	182.07	213.33	0.853
640	98.93	248.73	347.67	0.715	30.03	172.30	202.33	0.852
650	88.03	253.63	341.67	0.742	29.40	163.93	193.33	0.848
660	96.50	235.50	332.00	0.709	29.57	156.77	186.33	0.841
670	113.67	219.33	333.00	0.659	30.50	149.50	180.00	0.831
680	109.67	239.67	349.33	0.686	30.97	143.70	174.67	0.823
690	76.67	287.00	363.67	0.789	31.27	139.73	171.00	0.817
700	44.23	313.77	358.00	0.876	31.87	134.13	166.00	0.808
710	27.90	310.10	338.00	0.917	32.33	129.67	162.00	0.800
720	20.97	302.03	323.00	0.935	33.00	124.67	157.67	0.791
730	17.63	296.03	313.67	0.944	33.80	119.53	153.33	0.780
740	15.87	291.13	307.00	0.948	36.47	113.87	150.33	0.757
750	14.87	287.13	302.00	0.951	38.63	109.03	147.67	0.738
760	14.27	283.40	297.67	0.952	41.37	105.97	147.33	0.719
770	14.63	278.03	292.67	0.950	47.13	98.87	146.00	0.677
780	14.20	274.80	289.00	0.951	60.00	84.33	144.33	0.584
790	13.13	271.87	285.00	0.954	81.83	69.50	151.33	0.459
800	13.67	267.33	281.00	0.951	91.03	79.63	170.67	0.467
810	13.83	264.17	278.00	0.950	72.20	119.80	192.00	0.624
820	13.90	259.10	273.00	0.949	70.00	93.00	163.00	0.571
830	12.87	256.80	269.67	0.952	96.60	55.07	151.67	0.363
840	12.47	254.20	266.67	0.953	148.67	20.00	168.67	0.119
850	13.60	252.07	265.67	0.949	186.33	32.67	219.00	0.149
860	12.37	253.30	265.67	0.953	174.33	103.67	278.00	0.373
870	11.33	257.00	268.33	0.958	147.00	125.33	272.33	0.460
880	10.25	258.75	269.00	0.962	118.33	127.67	246.00	0.519
890	9.18	258.49	267.67	0.966	84.97	140.03	225.00	0.622
900	10.10	246.24	256.33	0.961	41.30	150.03	191.33	0.784

Table 1 (Continued)

λ (nm)	<i>A. variabilis</i>				<i>R. sphaeroides</i>			
	$A_{\text{abs},\lambda}$ (m ² /kg)	$S_{\text{sca},\lambda}$ (m ² /kg)	$E_{\text{ext},\lambda}$ (m ² /kg)	ω	$A_{\text{abs},\lambda}$ (m ² /kg)	$S_{\text{sca},\lambda}$ (m ² /kg)	$E_{\text{ext},\lambda}$ (m ² /kg)	ω
910	11.73	235.27	247.00	0.953	19.80	133.20	153.00	0.871
920	11.67	230.67	242.33	0.952	19.47	100.53	120.00	0.838
930	11.37	226.97	238.33	0.952	17.57	91.77	109.33	0.839
940	11.67	225.33	237.00	0.951	18.57	83.40	101.97	0.818
950	11.60	220.40	232.00	0.950	19.40	75.67	95.07	0.796
960	11.23	220.10	231.33	0.951	17.20	76.23	93.43	0.816
970	10.90	217.10	228.00	0.952	16.23	73.13	89.37	0.818
980	10.96	213.04	224.00	0.951	17.53	66.10	83.63	0.790
990	10.86	210.47	221.33	0.951	17.13	67.00	84.13	0.796
1000	10.71	206.63	217.33	0.951	15.67	64.73	80.40	0.805
1010	10.60	202.40	213.00	0.950	15.77	61.70	77.47	0.796
1020	10.70	198.30	209.00	0.949	16.67	56.90	73.57	0.773
1030	10.87	193.47	204.33	0.947	16.83	56.30	73.13	0.770
1040	10.60	189.40	200.00	0.947	15.93	52.60	68.53	0.768
1050	10.37	186.30	196.67	0.947	15.47	53.33	68.80	0.775
1060	10.26	182.41	192.67	0.947	15.33	49.17	64.50	0.762
1070	10.07	179.27	189.33	0.947	14.80	49.57	64.37	0.770
1080	10.03	175.97	186.00	0.946	14.70	46.97	61.67	0.762
1090	10.77	173.23	184.00	0.941	14.93	46.33	61.27	0.756
1100	10.39	171.61	182.00	0.943	14.70	45.43	60.13	0.756
1110	10.16	169.84	180.00	0.944	15.73	43.40	59.13	0.734
1120	10.67	168.00	178.67	0.940	14.73	43.73	58.47	0.748
1130	10.55	166.12	176.67	0.940	14.23	43.33	57.57	0.753
1140	10.40	166.60	177.00	0.941	14.60	43.10	57.70	0.747
1150	10.77	169.23	180.00	0.940	15.27	45.07	60.33	0.747
1160	10.97	170.37	181.33	0.940	15.50	43.07	58.57	0.735
1170	10.73	169.93	180.67	0.941	15.43	42.63	58.07	0.734
1180	10.53	167.80	178.33	0.941	15.33	41.37	56.70	0.730
1190	10.23	165.10	175.33	0.942	15.47	39.07	54.53	0.716
1200	10.17	163.17	173.33	0.941	15.27	37.47	52.73	0.710
1210	10.03	161.31	171.33	0.941	14.60	37.83	52.43	0.722
1220	10.08	158.58	168.67	0.940	14.50	35.93	50.43	0.712
1230	10.22	156.11	166.33	0.939	14.63	34.00	48.63	0.699
1240	10.33	153.33	163.67	0.937	14.20	33.50	47.70	0.702
1250	10.10	151.57	161.67	0.938	14.53	32.33	46.87	0.690
1260	10.05	149.62	159.67	0.937	15.17	31.03	46.20	0.672
1270	10.20	147.46	157.67	0.935	14.17	30.77	44.93	0.685
1280	9.44	147.56	157.00	0.940	12.43	33.03	45.47	0.727
1290	8.70	146.96	155.67	0.944	14.00	31.40	45.40	0.692
1300	9.58	145.08	154.67	0.938	14.17	29.63	43.80	0.677

Finally, Figs. 11(a) and (b) show the scattering phase function of *A. variabilis* and of *R. sphaeroides* measured at 632.8 nm with the nephelometer previously described along with the HG phase function approximation. They indicate that the scattering by both microorganisms is mainly in the forward direction. The phase function measurements suggest that scattering is mainly in the forward. Note that for practical applications the bacteria concentration is typically large to ensure maximum CO₂ consumption and/or hydrogen production. Thus, while in-scattering term in the radiation transfer equation due to multiple scattering is important, precise knowledge of the phase function is not essential for large concentrations as established by Berberoglu et al. [21]. As a first order approximation, the phase function at wavelengths other than 632.8 nm could be assumed to be identical to that reported in Fig. 11. The Henyey–Greenstein asymmetry factor [12] was found to be 0.9752 for *A. variabilis*

and 0.9651 for *R. sphaeroides* indicating strongly forward scattering which is not expected to change significantly within the wavelength range of interest.

5. Conclusions

This paper presents the complete set of radiation characteristics of two of the most promising hydrogen producing microorganisms. For the first time, a consistent set of radiation characteristics of both randomly oriented filamentous cyanobacteria *A. variabilis* and unicellular purple bacteria *R. sphaeroides* have been measured over the spectral range from 300 to 1300 nm. The reported radiation characteristics can be used to model photobioreactors or natural environments containing these microorganisms or can be used as a first order approximation to model systems involving other unicellular purple or filamentous

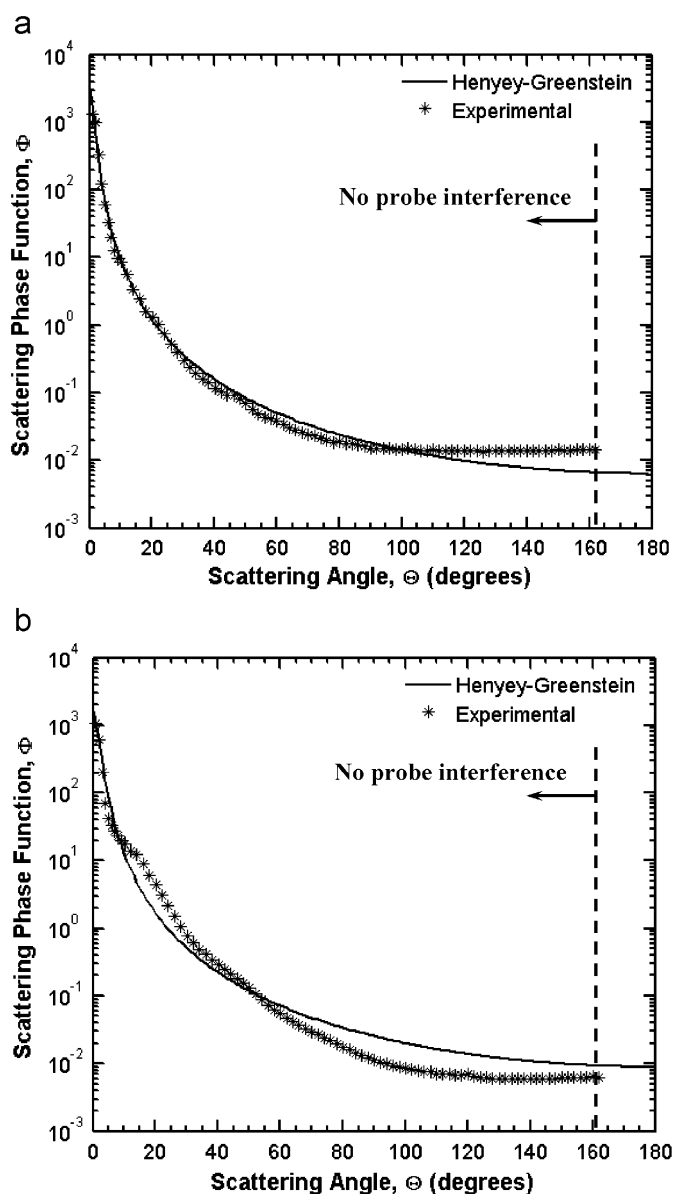


Fig. 11. Experimentally measured scattering phase function of (a) *A. variabilis* and (b) *R. sphaeroides* at 632.8 nm.

blue-green microorganisms. Moreover, the experimental methods presented here can be used to accurately measure the radiation characteristics of other microorganisms.

Acknowledgments

The authors gratefully acknowledge the support of the California Energy Commission through the Energy Innovation Small Grant (EISG 53723A/03-29; Project Manager: Michelle McGraw). They are indebted to Prof. J. Jay, Dr. T. Semenic and Dr. I. Martini for their helpful discussions and exchanges of information.

References

[1] Pulz O. Photobioreactors: production systems for phototrophic microorganisms. *Appl Microbiol Biotechnol* 2001;57(3):287–93.

- [2] Kim NJ, Suh IS, Hur BK, Lee CG. Simple monodimensional model for linear growth rate of photosynthetic microorganisms in flat-plate photobioreactors. *J Microbiol Biotechnol* 2002;12:962–71.
- [3] Markov SA, Lichtl R, Rao KK, Hall DO. A hollow fibre photobioreactor for continuous production of hydrogen by immobilized cyanobacteria under partial vacuum. *Int J Hydrogen Energy* 1993;18:901–6.
- [4] Markov SA, Bazin MJ, Hall DO. Hydrogen photoproduction and carbon dioxide uptake by immobilized *Anabaena variabilis* in a hollow-fiber photobioreactor. *Enzyme Microbiol Technol* 1995;17:306–10.
- [5] Markov SA, Thomas AD, Bazin MJ, Hall DO. Photoproduction of hydrogen by cyanobacteria under partial vacuum in batch culture or in a photobioreactor. *Int J Hydrogen Energy* 1997;22:521–4.
- [6] Tsygankov AA, Fedorov AS, Kosourov SN, Rao KK. Hydrogen production by cyanobacteria in an automated outdoor photobioreactor under aerobic conditions. *Biotechnol Bioeng* 2002;80:715–77.
- [7] Yoon JH, Shin JH, Kim MS, Sim SJ, Park TH. Evaluation of conversion efficiency of light to hydrogen energy by *Anabaena variabilis*. *Int J Hydrogen Energy* 2006;31:721–7.
- [8] Benemann JR. Hydrogen production by microalgae. *J Appl Phycol* 2000;12:291–300.
- [9] Cornet JF, Dussap CG, Dubertret G. A structured model for simulation of cultures of the cyanobacterium *Spirulina platensis* in photobioreactors: I. Coupling between light transfer and growth kinetics. *Biotechnol Bioeng* 1992;40:817–25.
- [10] Cornet JF, Dussap CG, Cluzel P, Dubertret G. A structured model for simulation of cultures of the cyanobacterium *Spirulina platensis* in photobioreactors: II. Identification of kinetic parameters under light and mineral limitations. *Biotechnol Bioeng* 1992;40:826–34.
- [11] Cornet JF, Dussap CG, Gross JB, Binois C, Lasseur C. A simplified monodimensional approach for modeling coupling between radiant light transfer and growth kinetics in photobioreactors. *Chem Eng Sci* 1995;50:1489–500.
- [12] Modest MF. Radiative heat transfer. San Diego, CA: Academic Press; 2003.
- [13] Stramski D, Morel A. Optical properties of picoplankton in different physiological states as affected by growth irradiance. *Deep Sea Res* 1990;37:245–66.
- [14] Kutser T, Metsamaa L, Strombeck N, Vahtmae E. Monitoring cyanobacterial blooms by satellite remote sensing. *Estuarine Coastal Shelf Sci* 2006;67:303–12.
- [15] Melis A, Happe T. Hydrogen production. Green algae as a source of energy. *Plant Physiol* 2001;127:740–8.
- [16] Melis A, Melnicki MR. Integrated biological hydrogen production. *Int J Hydrogen Energy* 2006;31:1563–73.
- [17] Sasikala K, Ramana CV, Rao PR. Environmental regulation for optimal biomass yield and photoproduction of hydrogen by *Rhodobacter sphaeroides* O.U 001. *Int J Hydrogen Energy* 1991;16:597–601.
- [18] Pinto FAL, Troshina O, Lindblad P. A brief look at three decades of research on cyanobacterial hydrogen evolution. *Int J Hydrogen Energy* 2002;27:1209–15.
- [19] Das D, Veziroğlu TN. Hydrogen production by biological processes: a survey of literature. *Int J Hydrogen Energy* 2001;26:13–28.
- [20] Agrawal BM, Mengüç MP. Forward and inverse analysis of single and multiple scattering of collimated radiation in an axisymmetric system. *Int J Heat Mass Transfer* 1991;34:633–47.
- [21] Berberoğlu H, Yin J, Pilon L. Simulating light transfer in a bubble sparged photobioreactor for simultaneous hydrogen fuel production and CO₂ mitigation. *Int J Hydrogen Energy* 2007;32:2273–85.
- [22] Daniel KJ, Incropera FP. Optical property measurements in suspensions of unicellular algae. Purdue University Technical Report, HTL 77-4; 1977.
- [23] Privoznik KG, Daniel KJ, Incropera FP. Absorption, extinction, and phase function measurements for algal suspensions of *Chlorella pyrenoidosa*. *J Quant Spectrosc Radiat Transfer* 1978;20:345–52.
- [24] Bohren CF, Huffman DR. Absorption and scattering of light by small particles. New York, NY: Wiley; 1998.
- [25] Butler WL. The chlorophylls. New York, NY: Academic Press; 1966.

- [26] Merzlyak MN, Naqvi KR. On recording the true absorption spectrum and scattering spectrum of a turbid sample: application to cell suspensions of cyanobacterium *Anabaena variabilis*. *J Photochem Photobiol B: Biology* 2000;58:123–9.
- [27] Latimer P, Eubanks CAH. Absorption spectrophotometry of turbid suspensions: a method of correcting for large systematic deviations. *Arch Biochem Biophys* 1962;98:274–85.
- [28] Stramski D, Mobley CD. Effect of microbial particles on oceanic optics: a database of single-particle optical properties. *Limnol Oceanogr* 1997;42:538–49.
- [29] Pottier L, Pruvost J, Deremetz J, Cornet JF, Legrand J, Dussap CG. A fully predictive model for one-dimensional light attenuation by *Chlamydomonas reinhardtii* in a torus photobioreactor. *Biotechnol Bioeng* 2005;91:569–82.
- [30] Robinson JP. *Current protocols in cytometry*. New York, NY: Wiley; 2001.
- [31] Berberoglu H, Barra N, Pilon L, Jay JA. Growth, CO₂ consumption and H₂ production of *Anabaena variabilis* ATCC 29413-U under different irradiances and CO₂ concentrations. *J Appl Microbiol* 2007 (in press).
- [32] Arnaud JA, Hubbard WM, Mandevil GD, Claviere BD, Franke EA, Franke JM. Technique for fast measurement of Gaussian beam parameters. *Appl Opt* 1971;10:2775–81.
- [33] Ma X, Lu JQ, Brock RS, Jacobs KM, Yang P, Hu XH. Determination of complex refractive index of polystyrene microspheres from 370 to 1610 nm. *Phys Med Biol* 2003;48:4165–72.
- [34] Malitson IH. Interspecimen comparison of the refractive index of fused silica. *J Opt Soc Am* 1965;55:1205–9.
- [35] Kang RJ, Shi DJ, Cong W, Cai ZL, Ouyang F. Dispersion of the optical constants of quartz and polymethyl methacrylate glasses. *Opt Commun* 2001;188:129–39.
- [36] Lee SC. Scattering phase function for fibrous media. *Int J Heat Mass Transfer* 1990;33:2183–90.
- [37] Madigan MT, Martinko JM. *Brock biology of microorganisms*. Upper Saddle River, NJ: Pearson Prentice-Hall; 2006.
- [38] Broglie RM, Hunter CN, Delepelair P, Niederman RA, Chua NH, Clayton RK. Isolation and characterization of the pigment–protein complexes of *Rhodospseudomonas sphaeroides* by lithium dodecylsulfate/polyacrylamide gel electrophoresis. *Proc Nat Acad Sci USA* 1980;77: 87–91.